Chemical Physics Letters 675 (2017) 56–62

Contents lists available at ScienceDirect

Chemical Physics Letters

journal homepage: www.elsevier.com/locate/cplett

Research paper

Absorption cross sections and kinetics of formation of AlO at 298 K

Juan Carlos Gómez Martín, Shane M. Daly, James S.A. Brooke, John M.C. Plane *

School of Chemistry, University of Leeds, Leeds LS2 9JT, UK

ARTICLE INFO

Article history:
Received 24 January 2017
In final form 27 February 2017
Available online 3 March 2017

Keywords:
Gas phase metal chemistry
Laser spectroscopy
Aluminium monoxide

ABSTRACT

The rate coefficient of the Al + O_2 reaction has been measured in a laser ablation-fast flow tube apparatus by monitoring atomic Al resonance absorption and AlO laser induced fluorescence (LIF). The rate constant has been found to be $k(298\ \mathrm{K}) = (1.68 \pm 0.24) \times 10^{-10}\ \mathrm{cm^3\ molecule^{-1}\ s^{-1}}$. Under conditions of near-stoichiometric conversion of Al into AlO, the absorption cross section of AlO at the bandhead of the $B^2\Sigma^+(v' = 0) \leftarrow X^2\Sigma^+(v'' = 0)$ transition has been determined to be $\sigma(298\ \mathrm{K}, 1\ \mathrm{hPa}) = (6.7 \pm 1.6) \times 10^{-15}\ \mathrm{cm^2\ molecule^{-1}}$ (0.003 nm resolution), in very good agreement with theoretical predictions.

1. Introduction

The ablation of $\sim 40\ \mathrm{t\ d^{-1}}$ of cosmic dust particles in the mesosphere-lower thermosphere [1] results in the formation of metal layers, which are useful probes of the chemistry and dynamics of this region of the atmosphere and precursors to other atmospheric phenomena [2]. Some of these layers are very well studied, e.g. Fe and Na [3,4], while the atmospheric ablation and chemistry of other elemental constituents of meteoroids such as Ca, Ni, and Al are less well understood. In particular, while atmospheric detections of Ca/Ca^+ [5] and Ni [6] have been reported, an Al layer has not been observed, despite the fact that the abundance of Al in cosmic dust particles is of a similar magnitude to that of Ca and Ni [7–10], and the wealth of aeronomic studies based on chemical release of aluminium vapours in the upper atmosphere [11,12].

There are two main reasons for the lack of observations of the meteoric Al layer. First, Al is a refractory element and ablates less efficiently than most other meteoric elemental constituents [1] and second, the ablated Al atoms react rapidly with the abundant atmospheric O_2 [13–15] and are converted to AlO:

$$\mathrm{Al + O_2 \rightarrow AlO + O} \quad (\Delta H = -14 \pm 9\ \mathrm{kJ\ mol^{-1}}) \qquad \text{(R1)}$$

where the enthalpy change (at 0 K) of R1 is experimental [16]. Note that a theoretical value of $-1 \pm 5\ \mathrm{kJ\ mol^{-1}}$, calculated using the Complete Basis Set (CBS-QB3) method [17], agrees within error (the expected theoretical uncertainty is taken from Montgomery et al. [18]). This theoretical method is then used to calculate the reaction enthalpies of reactions (R2) and (R3) below. Detecting a molecular species in the mesosphere (e.g. by the resonance lidar technique) is more challenging than detecting an atomic species of similar abundance, owing to orders of magnitude smaller transition probabilities between molecular states compared to atomic transitions. In fact, active detection of naturally occurring meteoric metal-bearing molecules has to be yet demonstrated, although chemiluminescence from FeO and NiO in the airglow spectrum has been reported [19,20].

Solar-pumped fluorescence from the $B^2\Sigma^+ \leftarrow X^2\Sigma^+$ transition of AlO after twilight aluminium release experiments in the upper atmosphere has been observed [21], which suggest that this transition could be also useful for detection of Al naturally deposited by meteoric ablation [11]. Radiative lifetimes of the AlO $B^2\Sigma^+$ state have been experimentally and theoretically determined [22–24] determined. The oscillator strength of the 0–0 band, which has the highest Frank-Condon factor in the B-X system [25], is $f_{00} = 0.027$ [22] (*cf.* $f = 0.022$ for the Fe transition at 385.99 nm used in Doppler lidar measurements [26]). The peak of the 0–0 band at 484.23 nm consists of densely overlapped high and low J lines [27,28], and hence is expected to be strong and relatively temperature insensitive between 120 and 240 K, which makes it potentially suitable for AlO lidar measurements. Because of the astronomical relevance of AlO, theoretical spectra of the B-X transition based on measured molecular constants are available [24]. However, no experimental measurements of the absorption cross section of AlO have been carried out to validate these modelled spectra.

In this letter we report the first measurement of the absorption cross section of AlO at the bandhead of the B(0)-X(0) transition. A pre-requisite for this measurement is the characterisation of the chemical system, which involves determining the rate constant of R1. Two measurements of k_1 using the Pulsed Laser Photolysis – Laser Induced Fluorescence (PLP-LIF) technique agree well with

* Corresponding author.
E-mail address: J.M.C.Plane@leeds.ac.uk (J.M.C. Plane).

http://dx.doi.org/10.1016/j.cplett.2017.02.087
0009-2614/

each other [13,14], but disagree with the only published flow tube study [15].

2. Experiment

Fig. 1 is a schematic diagram of the Laser Ablation-Fast Flow Tube (LA-FFT) experimental set up. The majority of this system has been described in detail previously [29–31], and therefore we will focus here on modifications introduced in order to measure the absorption cross sections. Pulsed 532 nm Nd:YAG laser (Continuum Minilite) ablation of a rotating Al cylindrical target was used to entrain Al atoms in a flow of a carrier gas, typically 3 slm of N_2 at 0.7 Torr. A flow of O_2 was added downstream of the ablation source via a movable injector. The concentration of O_2 was changed by varying its flow while keeping the total flow constant by balancing with a flow of N_2. Contact times between O_2 and Al atoms were varied between 0.5 and 2.5 ms by changing the reagent injection point.

Al atoms were detected by Atomic Resonance Absorption Spectroscopy (ARAS), whereby the absorption of the 396.15 nm line of Al ($^2S_{1/2} \leftarrow {}^2P^\circ_{3/2}$) emitted by a hollow cathode lamp (Perkin Elmer) by the colder atoms in the flow tube along one single pass was detected using a monochromator (resolution 1.9 nm FWHM) and a photomultiplier (PMT) (Hamamatsu H7710-12). AlO absorption and fluorescence were measured by passing through the same optical port pulsed laser radiation generated by a Nd-YAG pumped dye laser (Continuum Surelite – Sirah Cobra Stretch) running on a solution of Coumarin 102 in ethanol, which spans the spectral range between 455 and 495 nm. The laser pulse width is 6 ns, with a linewidth of 0.003 nm. A flip mirror was used to alternate between the lamp and the laser beams. AlO fluorescence was collected perpendicularly to the excitation beam through a set of interference filters and lenses by a PMT (Electron Tubes, 9816QB). Resonance fluorescence from the B(0)-X(0) and B(1)-X(1) bands was observed using a band-pass filter centered at 482 nm (Ealing 35-3441, 10 nm FWHM). The transmission curve of the filter was measured using a UV–VIS absorption spectrometer (Perkin Elmer, Lambda 900). Off-resonance fluorescence was also observed through a yellow high pass filter (Comar 495GY25, cut-off at 495 nm) by pumping the aforementioned transitions, either B(1)-X(0) or B(2)-X(1). Resonance detection of AlO at B(0)-X(0) was used in the kinetic study because it gave better signal (even with the 25% peak transmission band pass filter), so that scattered light from the excitation laser was two orders of magnitude smaller than fluorescence. Intense fluorescence was collected from all the transitions scanned with the excitation laser, and in fact care had to be taken to avoid saturation of the PMT at the bandhead of the 0–0 transition by keeping the voltage of the PMT low (~800 V) and reducing the laser energy to ~0.5 mJ.

To compensate for the small diameter of the flow tube (3.75 cm), the laser beam was folded back and forth several times using mirrors to increase the AlO absorption pathlength. The laser pulse energy exiting this optical multi-pass arrangement was then monitored through a stack of neutral density filters by a PMT (Electron Tubes, 9816QB). The incident laser energy was monitored using a beamsplitter and photodiode, so that the PMT signal could be corrected for the pulse-to-pulse laser variability. A wavemeter (Coherent Wavemaster) calibrated to better than 3 decimal digits at the HeNe laser wavelength was used to monitor the wavelength of the dye laser beam during spectral scans.

A Time-of-Flight Mass Spectrometer with electron impact ionization (Kore Technology) was coupled to the end of the flow tube to assist in the identification of reaction products. The signals from the different detectors were recorded using a digital oscilloscope

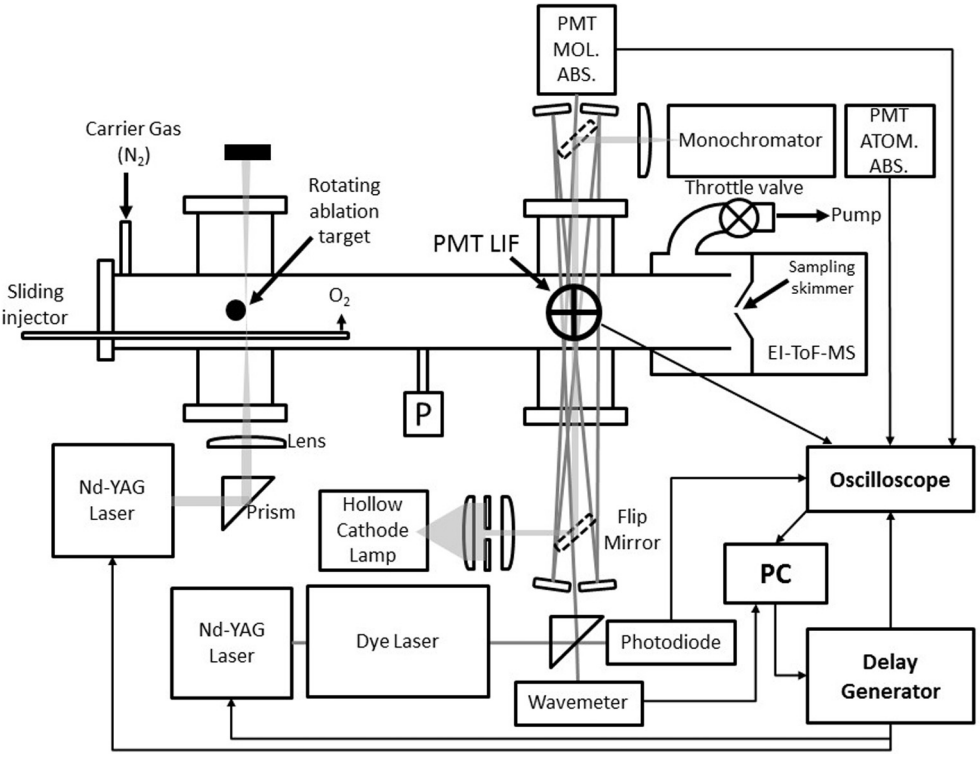

Fig. 1. The LA-FFT apparatus combining atomic resonance absorption and molecular laser induced fluorescence. Kinetic experiments are carried out by monitoring back-to-back AlO LIF and Al absorption under different O_2 concentrations and injection distances. A flip mirror is used to alternate between Al and AlO measurements. AlO LIF is collected by the PMT perpendicular to the plane of the diagram. Al absorption is detected by monitoring the 396.152 nm line of Al emitted by the lamp. AlO absorption from its B-X electronic transition is measured using a multi-pass arrangement. A mass spectrometer is attached at the end of the flow tube for ancillary measurements of reaction products. Pressure is measured by a calibrated pressure transducer (P). Flows of N_2 and O_2 are set via calibrated mass flow controllers.

(LeCroy LT342) and transferred to a computer for further analysis. The laser triggering, oscilloscope data acquisition and cycle repetition were synchronized using a delay generator.

2.1. Materials

OFN N_2 (BOC) was used as carrier gas. UHP O_2 (BOC) was used directly from the cylinder or from a glass bulb containing O_2 diluted in N_2 to a set partial pressure. A rod (diameter = 6 mm of industrial grade Al was machined to serve as the ablation target.

3. Results

An example of a set of back-to-back LIF and ARAS measurements for fixed contact time and varying O_2 concentration is shown in Fig. 2. Al atoms are removed and AlO formed concomitantly as O_2 is increased. For higher O_2 concentrations or longer contact times, the AlO LIF signal is also observed to decrease. The AlO growth curves showing decay (e.g. Fig. 2) were analyzed by fitting a bi-exponential expression with pseudo-first order growth and decay terms:

$$[\mathrm{AlO}] = [\mathrm{Al}](\exp(-k'_{\mathrm{AlO\ decay}}[\mathrm{O_2}]) - \exp(-k'_{\mathrm{AlO\ growth}}[\mathrm{O_2}])) \quad (E1)$$

where [AlO] and [Al] are concentrations at the detection region. A rate k' is defined in this context as the product of a rate constant and the contact time: $k' = k \times t$, in units of cm^3 $molecule^{-1}$. The underlying assumption in Eq. (E1) is that Al and AlO have a similar diffusion rate in N_2 to the flow tube walls (observed to be of the order of 300 s^{-1} for Al at 0.8 Torr). For datasets showing decay, only the first section of the decay was included in the fits, since overall the traces do not exhibit single exponential behavior, but the early decay can be approximated by a first order loss. E1 reduces into a single term describing AlO growth when the k'_{decay} term is set to 0 for traces not showing decay (i.e. short contact time). The rate constant of R1 is determined by regressing linearly the growth rates against contact time t:

$$k' = k_1 \times t + c \quad (E2)$$

The contact time can be calculated from the injection distance and the flow and pressure readings, taking into account the parabolic flow correction. Calculated times agree within better than 5% with the observed flight time of the Al and AlO pulses between the ablation and the detection regions. Fig. 3 shows the plot of k'_{growth} vs contact time (triangles), where the linear fit (dashed line) shows intercept zero within error and a slope of $(1.73 \pm 0.26) \times 10^{-10}$ cm^3 $molecule^{-1}$ s^{-1}.

The empirical first order decay rates derived from fitting E1 to the data result in apparent rate constants which are faster by a factor of five or higher than would be expected from the reaction:

$$\mathrm{AlO} + \mathrm{O_2} + \mathrm{M} \rightarrow \mathrm{AlO_3} + \mathrm{M} \quad (\Delta H = -218\ \mathrm{kJ\ mol^{-1}}) \quad (R2)$$

The rate constant at 0.8 Torr and 298 K calculated from the Troe expression published for R2 [32] is $k_2 = 1 \times 10^{-13}$ cm^3 $molecule^{-1}$ s^{-1}. Fig. 2 shows that this value (thin dashed line) does not account for the observed removal of AlO, which would require k_2 to be 4.6 times faster (thick dashed line). Also, the effective removal rates $k'_{\mathrm{AlO\ decay}}$ are contact time dependent. This suggests that other process may dominate the removal of AlO, e.g. the AlO self-reaction:

$$\mathrm{AlO} + \mathrm{AlO} \rightarrow \mathrm{Al_2O} + \mathrm{O} \quad (\Delta H = -70\ \mathrm{kJ\ mol^{-1}}) \quad (R3a)$$

$$+ \mathrm{M} \rightarrow \mathrm{Al_2O_2} + \mathrm{M} \quad (\Delta H = -516\ \mathrm{kJ\ mol^{-1}}) \quad (R3b)$$

In fact, addition of O_2 resulted in the appearance of $m/z = 70$ in the mass spectra (electron impact energy = 70 eV), which suggests that channel R3a dominates. Reaction (R3) with an assumed rate constant of $\sim 3 \times 10^{-10}$ cm^3 $molecule^{-1}$ s^{-1} would explain the first section of the observed decays for $[O_2] < 5 \times 10^{13}$ molecule cm^{-3}. However, a secondary removal process needs to be invoked for larger $[O_2]$. Some evidence of clustering was found in the mass spectra, where $m/z = 97$ (Al_3O^+) is the only other peak (possibly a fragment) that stands out alongside $m/z = 70$ (see Fig. S2 in the Supplementary Information). This possibly starts by AlO reacting

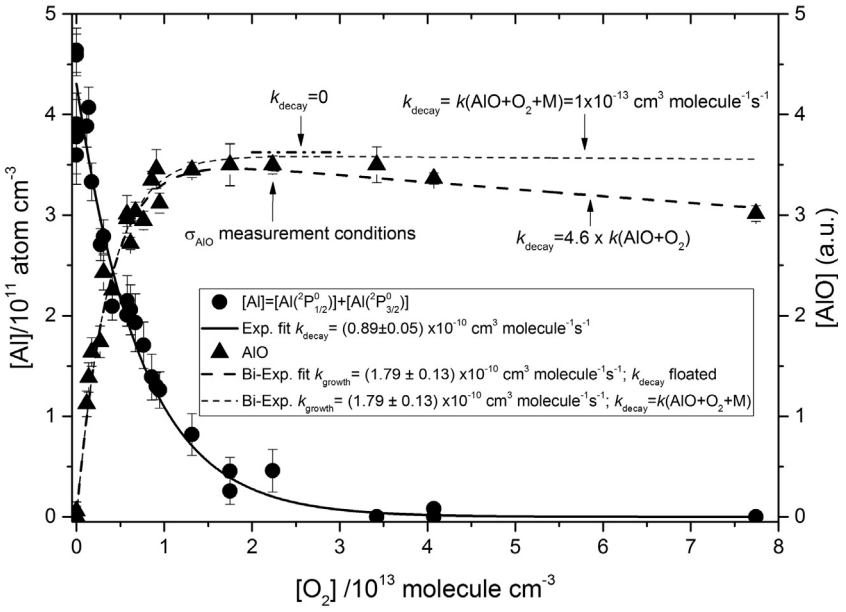

Fig. 2. Al decay (circles) and AlO formation (triangles) for increasing O_2 concentration and at a fixed contact time of 1.5 ms. The growth rate of the AlO LIF signal is faster than the rate of decay of the Al absorption signal, because the former is measured at the well mixed core of the laminar flow, while the latter is measured across the flow tube diameter, being the time scale for radial diffusion of O_2 of the same order of the experiment contact time (see Fig. 3). The thick dashed line is a bi-exponential fit where the AlO decay rate is floated, and the short dashed thick line indicates the maximum AlO if there was no decay. The thin dashed line is an evaluation of the bi-exponential expression E1 with the AlO growth rate found in the fit and a decay rate given by the estimated rate constant of AlO + O_2 at 0.8 Torr [32].

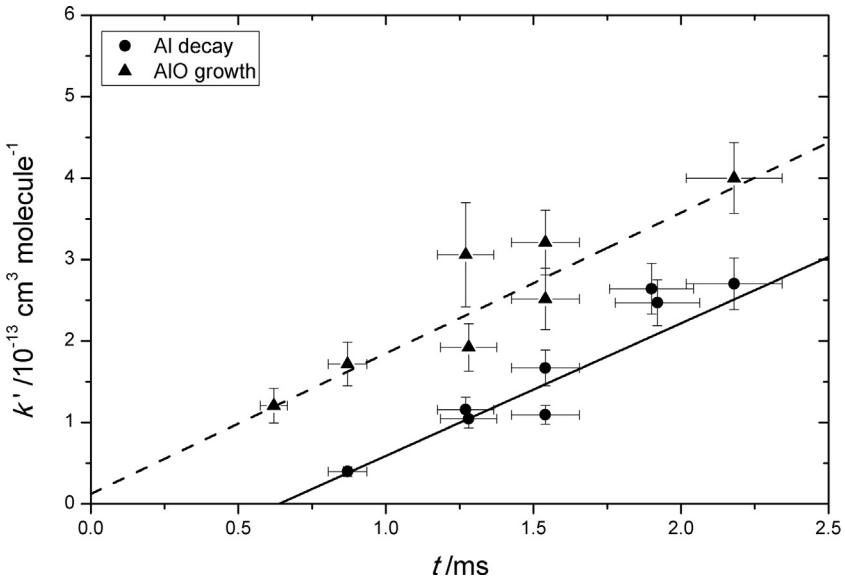

Fig. 3. Bimolecular plot for Al + O_2. The AlO growth and Al decay rates (triangles and circles respectively) derived from fits as those shown in Fig. 2 are plotted against contact time. The rate constant of the reaction is given by the slope obtained from weighted least squares linear regression (dashed line for AlO, solid line for Al). The non-zero intercept of the Al scatterplot reflects the radial mixing time of O_2 in the laminar flow.

with a product of its self-reaction, but the available data is insufficient to shed light into these processes and therefore no further efforts were made to model the AlO decays.

The ARAS data is analyzed following the standard method of equating the observed relative absorption $(I_0 - I)/I_0$ to the difference of integrated absorption and emission line profiles, where the exponential dependence of the absorption coefficient is approximated by a Taylor series [33,34]. The Doppler temperature of the commercial Al hollow cathode lamp is assumed to be 600 K, as documented in previous studies [35–37]. The procedure yields values of column density ($L \times$ [Al], where $L \sim 3.75$ cm is the optical path for one single pass). Fig. 2 shows an example of the Al atom decay corresponding to the overlaid AlO growth, where for clarity the column density has been scaled to concentration using the flow tube diameter. The Al decays are well fitted by single exponential decays, but the decay constants are smaller than the corresponding growth constants. By plotting the Al decay rates vs contact time and fitting to E2, it can be seen (Fig. 3, circles and solid line) that the slope of the liner regression is very close to that obtained from the AlO growth: $(1.63 \pm 0.22) \times 10^{-10}$ cm^3 molecule^{-1} s^{-1}, but the intercept is non-zero ($c = 0.75$ ms). This reflect the existence of a mixing time of the O_2 into the laminar flow. In other words, the radial diffusion time of O_2 is of the same order as the contact time. The LIF arrangement collects fluorescence from the core of the laminar flow, where mixing has been achieved quickly after O_2 injection, and therefore the AlO growth is not affected by diffusion. Al absorption by contrast samples across the whole flow tube diameter, averaging the Al concentration at the core and the outer laminae of the flow where the O_2 concentration is lower. Nevertheless, the *k'* vs contact time allows correcting for this, in a similar manner to the way in which a background removal process is accounted for by the intercept of a bimolecular plot in the time-resolved PLP-LIF technique. The average rate constant obtained using the LIF and ARAS datasets is $k_1(298\ \text{K}) = (1.68 \pm 0.24) \times 10^{-10}$ cm^3 molecule^{-1} s^{-1} (1σ).

Previous to the absorption experiments, B(0)-X(0) resonance fluorescence was recorded as a function of excitation laser wavelength (solid line in Fig. 4). The spectrum was normalized to the measured dye efficiency and filter transmission curves. The spectral efficiency of the PMT does not change significantly in the narrow spectral range of the measurements. The absorption spectrum in Fig. 4 was recorded under the conditions indicated in Fig. 2, with 5 passes through the flow tube: 1000 spectra were normalized to the corresponding laser energy spectra and co-added. Despite the challenging task of registering molecular absorption with a pulsed laser, the absorption band emerged from the noise at the expected wavelength range indicated by the LIF spectrum. Additional measurements were carried out with the dye laser fixed at the 0–0 bandhead and the ablation laser was switched on and off with a continuous O_2 flow. As shown in the insert of Fig. 4, the transmitted intensity decreased when the ablation started, indicating the appearance of AlO. The absorption cross section of AlO at 482.321 nm was determined using the Beer-Lambert law and considering the near-stoichiometric conversion of Al into AlO:

$$\sigma_{\text{AlO}} = \frac{\text{OD}}{n \times L \times [\text{AlO}]} = \frac{\ln(I_0/I)}{n \times L \times [\text{Al}] \times \phi} \qquad \text{(E3)}$$

where OD = ln (I_0/I) is the optical density of AlO, I_0 and I are the laser intensities transmitted through the tube without and with AlO respectively, n is the number of passes of the laser beam through the tube, $L \times$ [Al] is the column density of ground state Al atoms in the absence of O_2 measured by ARAS, and ϕ is a factor encompassing the loss of AlO by other processes (R2 and R3) and the aforementioned incomplete conversion of Al into AlO due to slow diffusion of O_2 towards the outer laminae of the flow. This method is convenient because it allows to by-pass the problem of determining the optical path length, with the caveat of the incomplete Al removal that we have discussed above, which needs to be corrected for.

In the absence of O_2 and for the flow and pressure conditions of the absorption experiments, the column density of Al($^2P_{3/2}$) measured at 392.15 nm is calculated to be $L \times [\text{Al}(^2P_{3/2})] = (8.0 \pm 1.4) \times 10^{11}$ atom cm^{-2}. At 289 K, the equilibrium populations of the Al ground state doublet are 0.46 for $J = 1/2$ and 0.54 for $J = 3/2$. Therefore, $L \times [\text{Al}] = L \times [\text{Al}\ (^2P^\circ_{1/2}) + \text{Al}\ (^2P^\circ_{3/2})] = (1.47 \pm 0.25) \times 10^{12}$ atom cm^{-2}, where the uncertainty includes the scatter in the observed atomic absorption and the estimated Doppler temperature range (450–750 K). The kinetic plots (e.g. Fig. 2) are used to estimate the fraction of Al across the absorption

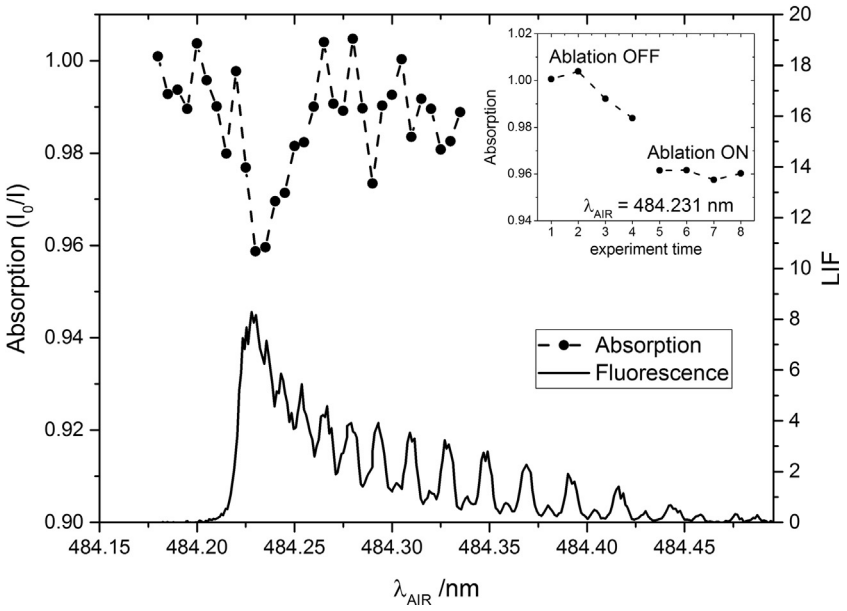

Fig. 4. Absorption through the flow tube (circles) as a function of wavelength around the band-head of the B(0)-X(0) band of AlO. The corresponding LIF spectrum is also plotted (solid line). The insert shows the drop in transmitted intensity at a fixed wavelength occurring when the ablation laser is turned on.

path that has not been converted into AlO, and how much AlO has been lost by secondary processes; this yields $\phi = 0.76 \pm 0.06$. With $OD(\lambda_{air} = 484.23\ nm) = 0.037 \pm 0.005$ from Fig. 4, the resulting absorption cross section is $\sigma(\lambda_{air} = 484.23\ nm) = (6.7 \pm 1.6) \times 10^{-15}\ cm^2\ molecule^{-1}$ (0.0027 nm resolution).

4. Discussion

The first measurement of k_1 as a function of temperature was carried out by Fontijn and co-workers [15] using absorption and resonance fluorescence detection of Al in a High Temperature Fast Flow Reactor (HTFFR) experiment, reporting a value of $k_1 = 3.2 \times 10^{-10}\ cm^3\ molecule^{-1}\ s^{-1}$ at 298 K. Two subsequent measurements using the PLP-LIF technique in a conventional slow flow reactor [13], and in a CRESU apparatus [14], reported the rate constant at 298 K to be $\sim 1.7 \times 10^{-10}\ cm^3\ molecule^{-1}\ s^{-1}$. Fontijn and co-workers agreed subsequently that their first measurement of k_1 was in error [13,38]. Our result is in excellent agreement with the two PLP-LIF determinations of the rate constant of k_1 at 298 K, showing once again that laser ablation provides a reliable atom source for fast flow tube experiments.

Rate theory calculations of the rate constant of the $AlO + O_2$ recombination reaction (R2) using the master equation solver MESMER [39] have been carried out with the required AlO_3 bond energy and molecular constants derived from ab initio calculations (see Table S1) [40,41]. The Inverse Laplace Transform method was used, with the high pressure limit rate constant given by the long-range capture rate constant [42]. Without tuning any parameter, the calculation agrees within a factor of 3 with the value of k_2(298, 0.8 Torr) obtained from the expressions reported by Belyung and Fontijn [32], which increases confidence in their experimental determination of k_2. Therefore, the observed removal of AlO cannot result from R2, as shown in Fig. 2. The relatively high concentrations of Al at the core of the flow ($\sim 1.2 \times 10^{12}\ cm^{-3}$ at the ablation region and $6 \times 10^{11}\ cm^{-3}$ at the observation point in the absence of O_2) suggest that if the AlO self-reaction (R3) proceeds at the gas kinetic collision rate, it may be partly responsible for this removal. In fact, owing to the large dipole moment of AlO (4.36 D), the dipole-dipole capture rate constant at 298 K is also large ($1.1 \times 10^{-9}\ cm^3\ molecule^{-1}\ s^{-1}$). We have carried out electronic structure calculations at the B3LYP/6-311+(2d,p) level of theory [17] on the potential energy surface of R3, which does not show a barrier between the linear Al_2O_2 adduct and the $Al_2O + O$ exit channel (Fig. S3). Thus, R3 is likely to proceed via channel R3a, which is consistent with the mass spectrometric detection of Al_2O. However, numerical modelling shows that the AlO decays are more complex and faster than second order in AlO (Fig. S1). Since an Al_3O^+ signal is also observed in the mass spectrum (Fig. S2), the AlO removal may also involve clustering reactions, but the dependence on $[O_2]$ and the speed of the removal are difficult to explain. We have no mass spectrometric evidence of any impurities that could be interfering with the measurements.

The $B^2\Sigma^+ \leftarrow X^2\Sigma^+$ transition of AlO has been extensively studied in the past and it is spectroscopically well understood [22,25,27,28,43]. Molecular constants for many low-lying vibrational states in the ground and the B excited states are available [44]. Several theoretical studies have also reported calculated transition dipole moments [23,24], corresponding to radiative lifetimes in agreement with experimental observations. We have used the molecular constants evaluated by Launila and Berg [44], potential energy functions calculated using RKR1 [45], vibrational wavefunctions from the Schrödinger equation solver LEVEL16 [46] and the B-X transition dipole moment function calculated by Patrascu et al. [24] to compute synthetic spectra of AlO at 298 K with the PGOPHER spectral simulator [47], in order to compare to the LIF spectra recorded in the present study under strictly thermal conditions at 298 K and moderate resolution (0.003 nm or 0.12 cm^{-1}) and pressure ($\sim$1 hPa). These experimental conditions are much closer to those in the mesospheric environment than in the typical flame and discharge sources used in previous spectroscopic studies.

Spectra of the 0–0 and the 1–0 bands are shown in Fig. 5 alongside the corresponding simulations. The best match is obtained by convolving the simulated spectra with a Gaussian with 0.18–0.25 cm^{-1} FWHM, which accounts for Doppler broadening and spectral resolution. The calculated cross section at the head of the 0–0 band (top panel) is $8.5 \times 10^{-15}\ cm^2\ molecule^{-1}$, in good agreement with the absorption cross section measured in this work. The measured LIF spectrum of the 0–0 band has been scaled

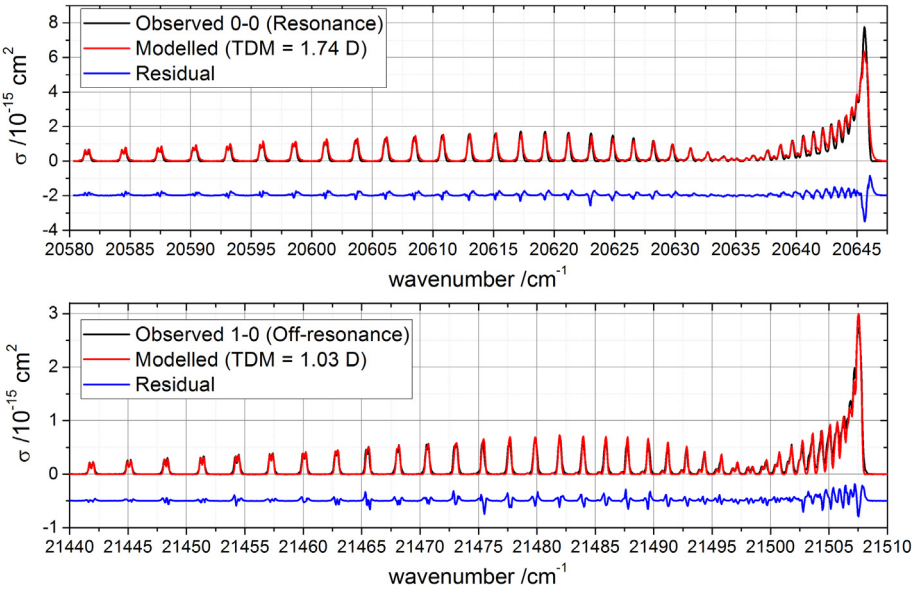

Fig. 5. Top: measured and calculated B(0)-X(0) band of AlO, and the residual (measured–simulated). Bottom: the same for the B(1)-X(0) band. The calculated transition dipole moments (TDM) for both vibrational bands are indicated.

to the experimental absorption cross section. The disagreement at the bandhead and the sharp flank of the R branch, as well as other features remaining in the residual, appear to result from deviations of actual line broadening from a simple Gaussian convolution. The observed lines have long wings, which can be approximated by increasing the Gaussian width or by including a small Lorentz component, but then the spin-orbit doubling of the P branch lines is lost. The 1–0 band (bottom) is very well fitted by PGOPHER. Both spectra appear fully thermalized.

The excellent agreement with the relative intensities across the whole of the 1–0 band gives confidence in the use of PGOPHER for generating reference spectra for atmospheric and astrochemical purposes, provided that the instrument line shape is well characterized. The simulated spectra also show very little change of the band head cross section between 200 K and 298 K as expected (Fig. S4), which is helpful for the purpose of atmospheric retrieval of absolute AlO densities. The peak cross section at the bandwidth of 0.003 nm, not far from typical lidar bandwidths, is very large compared to other diatomics -in fact it is *only* ~80 times smaller than the cross section of the Fe line used for mesospheric lidar retrievals. Assuming the AlO layer peak density is around 1000 cm^{-3} (based on the relative Fe/Al abundance in micrometeoroids) the expected AlO resonant backscatter is equivalent to ~12 Fe atom cm^{-3}, which are detectable with 1 min of signal-averaging with a state-of-the-art Fe lidar [26].

5. Conclusions

The rate constant of the Al + O_2 reaction can be considered now as firmly stablished. Evidence has been found for the AlO self-reaction, which appears to be faster than the gas kinetic collision rate -arguably because of the large dipole moment of AlO- and proceeds via the Al_2O + O product channel. The absorption cross section of AlO has been found to be $\sigma = (6.7 \pm 1.6) \times 10^{-15}$ cm^2 $molecule^{-1}$ at 298 K and 0.8 Torr (0.003 nm resolution). This is the first measurement of this parameter. The ro-vibrational spectral model PGOPHER with evaluated molecular constants of AlO reproduces the cross section at the 0–0 band head satisfactorily. PGOPHER also reproduces very well the intensities of the rotational lines, which gives confidence in its use to generate reference spectra and to understand the temperature dependence of cross sections. Our results are promising for a potential atmospheric detection of meteoric AlO by lidar.

Acknowledgements

This work was supported by the Natural Environment Research Council (grant number NE/P001815/1) and the European Research Council (project number 291332 – CODITA). SMD has a research studentship funded by the NERC's SPHERES doctoral training programme.

Appendix A. Supplementary material

Supplementary data associated with this article can be found, in the online version, at http://dx.doi.org/10.1016/j.cplett.2017.02.087.

References

[1] J.D. Carrillo-Sánchez, D. Nesvorný, P. Pokorný, D. Janches, J.M.C. Plane, Sources of cosmic dust in the Earth's atmosphere, Geophys. Res. Lett. 43 (2016) 11.
[2] J.M.C. Plane, W. Feng, E.C.M. Dawkins, The mesosphere and metals: chemistry and changes, Chem. Rev. 115 (2015) 4497.
[3] C.S. Gardner, A.Z. Liu, Y. Guo, Vertical and horizontal transport of mesospheric Na: implications for the mass influx of cosmic dust, J. Atmos. Sol. Terr. Phys. (2016), http://dx.doi.org/10.1016/j.jastp.2016.07.013.
[4] W. Huang, X. Chu, C.S. Gardner, J.D. Carrillo-Sánchez, W. Feng, J.M.C. Plane, D. Nesvorný, Measurements of the vertical fluxes of atomic Fe and Na at the mesopause: implications for the velocity of cosmic dust entering the atmosphere, Geophys. Res. Lett. 42 (2015) 169.
[5] G. Granier, J.P. Jégou, G. Mégie, Resonant lidar detection of Ca and Ca+ in the upper atmosphere, Geophys. Res. Lett. 12 (1985) 655.
[6] R.L. Collins, J. Li, C.M. Martus, First lidar observation of the mesospheric nickel layer, Geophys. Res. Lett. 42 (2015) 665.
[7] P. Arndt, J. Bohsung, M. Maetz, E.K. Jessberger, The elemental abundances in interplanetary dust particles, Meteorit. Planet. Sci. 31 (1996) 817.
[8] M.J. Genge, M.M. Grady, R. Hutchison, The textures and compositions of fine-grained Antarctic micrometeorites: implications for comparisons with meteorites, Geochim. Cosmochim. Acta 61 (1997) 5149.
[9] G. Kurat, C. Koeberl, T. Presper, F. Brandstätter, M. Maurette, Petrology and geochemistry of Antarctic micrometeorites, Geochim. Cosmochim. Acta 58 (1994) 3879.
[10] L.S. Schramm, D.E. Brownlee, M.M. Wheelock, Major element composition of stratospheric micrometeorites, Meteoritics 24 (1989) 99.

[11] J.L. Gole, C.E. Kolb, On the upper atmospheric chemiluminescent emission observed upon release of aluminum vapor and its compounds, J. Geophys. Res. [Space Phys.] 86 (1981) 9125.
[12] E.R. Johnson, Twilight resonance radiation of AlO in the upper atmosphere, J. Geophys. Res. 70 (1965) 1275.
[13] N.L. Garland, H.H. Nelson, Temperature dependence of the kinetics of the reaction Al + O_2 → AlO + O, Chem. Phys. Lett. 191 (1992) 269.
[14] S.D. Le Picard, A. Canosa, D. Travers, D. Chastaing, B.R. Rowe, T. Stoecklin, Experimental and theoretical kinetics for the reaction of Al with O_2 at temperatures between 23 and 295 K, J. Phys. Chem. A 101 (1997) 9988.
[15] A. Fontijn, W. Felder, J.J. Houghton, HTFFR kinetics studies. Temperature dependence of Al/O_2 and AlO/O_2 kinetics from 300 to 1700/1400 K, Symp. (Int.) Combust. 16 (1977) 871.
[16] R.D. Johnson III, NIST Computational Chemistry Comparison and Benchmark Database, NIST Standard Reference Database Number 101, 2016. <http://cccbdb.nist.gov>.
[17] M.J. Frisch, G.W. Trucks, H.B. Schlegel, G.E. Scuseria, M.A. Robb, J.R. Cheeseman, G. Scalmani, V. Barone, B. Mennucci, G.A. Petersson, H. Nakatsuji, M. Caricato, X. Li, H.P. Hratchian, A.F. Izmaylov, J. Bloino, G. Zheng, J.L. Sonnenberg, M. Hada, M. Ehara, K. Toyota, R. Fukuda, J. Hasegawa, M. Ishida, T. Nakajima, Y. Honda, O. Kitao, H. Nakai, T. Vreven, J.A. Montgomery Jr., J.E. Peralta, F. Ogliaro, M.J. Bearpark, J. Heyd, E.N. Brothers, K.N. Kudin, V.N. Staroverov, R. Kobayashi, J. Normand, K. Raghavachari, A.P. Rendell, J.C. Burant, S.S. Iyengar, J. Tomasi, M. Cossi, N. Rega, N.J. Millam, M. Klene, J.E. Knox, J.B. Cross, V. Bakken, C. Adamo, J. Jaramillo, R. Gomperts, R.E. Stratmann, O. Yazyev, A.J. Austin, R. Cammi, C. Pomelli, J.W. Ochterski, R.L. Martin, K. Morokuma, V.G. Zakrzewski, G.A. Voth, P. Salvador, J.J. Dannenberg, S. Dapprich, A.D. Daniels, Ö. Farkas, J.B. Foresman, J.V. Ortiz, J. Cioslowski, D.J. Fox, Gaussian 09, Gaussian Inc, Wallingford, CT, USA, 2009.
[18] J.A. Montgomery Jr., M.J. Frisch, J.W. Ochterski, G.A. Petersson, A complete basis set model chemistry. VI. Use of density functional geometries and frequencies, J. Chem. Phys 110 (1999) 2822.
[19] D.V. Saran, T.G. Slanger, W. Feng, J.M.C. Plane, FeO emission in the mesosphere: detectability, diurnal behavior, and modeling, J. Geophys. Res. 116 (2011) D12303.
[20] W.F.J. Evans, R.L. Gattinger, A.L. Broadfoot, E.J. Llewellyn, The observation of chemiluminescent NiO* emissions in the laboratory and in the night airglow, Atm. Chem. Phys. 11 (2011) 9595.
[21] D. Golomb, O. Harang, F.P. DelGreco, Upper atmosphere densities and temperatures at 105–165 kilometers from diffusion and spectral intensity of AlO trails, J. Geophys. Res. 72 (1967) 2365.
[22] P.J. Dagdigian, H.W. Cruse, R.N. Zare, Laser fluorescence study of AlO formed in the reaction Al + O_2: product state distribution, dissociation energy, and radiative lifetime, J. Chem. Phys 62 (1975) 1824.
[23] C. Zenouda, P. Blottiau, G. Chambaud, P. Rosmus, Theoretical study of the electronic states of AlO and AlO−, J. Mol. Struct. (Teochem.) 458 (1998) 61.
[24] A.T. Patrascu, S.N. Yurchenko, J. Tennyson, ExoMol molecular line lists – IX. The spectrum of AlO, Mon. Not. R. Astron. Soc. 449 (2015) 3613.
[25] C.T. Londhe, K. Sunanda, M.D. Saksena, S.H. Behere, Franck-Condon factors and r-centroids of B-X, C–X and C–A band systems of AlO molecule, J. Mol. Spectrosc. 263 (2010) 178.
[26] J. Lautenbach, J. Höffner, Scanning iron temperature lidar for mesopause temperature observation, Appl. Opt. 43 (2004) 4559.
[27] D. Kraus, R.J. Saykally, V.E. Bondybey, Cavity-ringdown spectroscopy studies of the $B^2\Sigma^+ \leftarrow X^2\Sigma^+$ system of AlO, Chem. Phys. Chem. 3 (2002) 364.
[28] M.D. Saksena, M.N. Deo, K. Sunanda, S.H. Behere, C.T. Londhe, Fourier transform spectral study of $B^2\Sigma^+$–$X^2\Sigma^+$ system of AlO, J. Mol. Spectrosc. 247 (2008) 47.
[29] J.C. Gomez Martin, J.M.C. Plane, Kinetic studies of atmospherically relevant silicon chemistry. Part III: Reactions of Si+ and SiO+ with O_3, and Si+ with O_2, Phys. Chem. Chem. Phys. 13 (2011) 3764.
[30] D.E. Self, J.M.C. Plane, A kinetic study of the reactions of iron oxides and hydroxides relevant to the chemistry of iron in the upper mesosphere, Phys. Chem. Chem. Phys. 5 (2003) 1407.
[31] J.C. Gómez Martín, S.A. Garraway, J.M.C. Plane, Reaction kinetics of meteoric sodium reservoirs in the upper atmosphere, J. Phys. Chem. A 120 (2016) 1330.
[32] D.P. Belyung, A. Fontijn, The AlO + O^2 reaction system over a wide temperature range, J. Phys. Chem. 99 (1995) 12225.
[33] J. Laimer, G. Misslinger, C.G. Schwärzler, H. Störi, Determination of atomic hydrogen densities in gases by a deuterium based Lyman-alpha absorption method, J. Appl. Phys. 80 (1996) 2060.
[34] P. Spietz, U. Gross, E. Smalins, J. Orphal, J.P. Burrows, Estimation of the emission temperature of an electrodeless discharge lamp and determination of the oscillator strength for the I(2P3/2) 183.038 nm resonance transition, Spectrochim. Acta, Part B 56 (2001) 2465.
[35] B.V. L'Vov, D.A. Katskov, L.P. Kruglikova, L.K. Polzik, Absolute analysis by flame atomic absorption spectroscopy: present status and some problems, Spectrochim. Acta, Part B 31 (1976) 49.
[36] V. Pavski, C.L. Chakrabarti, Atomic line profiles in hollow cathode lamps and a glow discharge atomizer determined by Fourier transform spectroscopy, Appl. Spectrosc. 49 (1995) 927.
[37] H.C. Wagenaar, I. Novotný, L. De Galan, The influence of hollow-cathode lamp line profiles upon analytical curves in atomic absorption spectroscopy, Spectrochim. Acta, Part B 29 (1974) 301.
[38] N.L. Garland, Gas Phase Metal Reactions, Elsevier, Amsterdam, 1992, p. 73.
[39] D.R. Glowacki, C.-H. Liang, C. Morley, M.J. Pilling, S.H. Robertson, MESMER: an open-source master equation solver for multi-energy well reactions, J. Phys. Chem. A 116 (2012) 9545.
[40] A.B.C. Patzer, C. Chang, E. Sedlmayr, D. Sülzle, A density functional study of small AlxOy (x, y = 1–4) clusters and their thermodynamic properties, Eur. Phys. J. D 32 (2005) 329.
[41] P. Politzer, P. Lane, M.E. Grice, Energetics of aluminum combustion, J. Phys. Chem. A 105 (2001) 7473.
[42] Y. Georgievskii, S.J. Klippenstein, Long-range transition state theory, J. Chem. Phys. 122 (2005) 194103.
[43] M.D. Saksena, G.S. Ghodgaonkar, M. Singh, The $B^2\Sigma^+$-$X^2\Sigma^+$ system of AlO, J. Phys. B: At., Mol. Opt. Phys. 22 (1989) 1993.
[44] O. Launila, L.E. Berg, Spectroscopy of AlO: combined analysis of the $A^2\Pi i \rightarrow X^2\Sigma^+$ and $B^2\Sigma^+ \rightarrow X^2\Sigma^+$ transitions, J. Mol. Spectrosc. 265 (2011) 10.
[45] R.J. Le Roy, RKR1: a computer program implementing the first-order RKR method for determining diatomic molecule potential energy functions, J. Quant. Spectrosc. Radiat. Transfer 186 (2017) 158.
[46] R.J. Le Roy, LEVEL: a computer program for solving the radial Schrödinger equation for bound and quasibound levels, J. Quant. Spectrosc. Radiat. Transfer 186 (2017) 167.
[47] C.M. Western, PGOPHER Version 9.1, 2016, p. University of Bristol Research Data Repository.